Åbo Akademi

OPEN ACCESS

This is an electronic reprint of the original article. This reprint may differ from the original in pagination and typographic detail.

Anisotropic ridge/groove microstructure for regulating morphology and biological function of Schwann cells

Li, Guicai; Zhao, Xueying; Zhang, Luzhong; Yang, Jian; Cui, Wenguo; Yang, Yumin; Zhang, Hongbo

Published in:
Applied Materials Today

DOI:
10.1016/j.apmt.2019.100468

Published: 01/01/2020

Document Version
Accepted author manuscript

Document License
CC BY

Link to publication

Please cite the original version:
Li, G., Zhao, X., Zhang, L., Yang, J., Cui, W., Yang, Y., & Zhang, H. (2020). Anisotropic ridge/groove microstructure for regulating morphology and biological function of Schwann cells. *Applied Materials Today*, *18*, Article 100468. https://doi.org/10.1016/j.apmt.2019.100468

General rights
Copyright and moral rights for the publications made accessible in the public portal are retained by the authors and/or other copyright owners and it is a condition of accessing publications that users recognise and abide by the legal requirements associated with these rights.

Take down policy
If you believe that this document breaches copyright please contact us providing details, and we will remove access to the work immediately and investigate your claim.

This document is downloaded from the Research Information Portal of ÅAU: 01. May. 2024

Anisotropic ridge/groove microstructure for regulating morphology and biological function of Schwann cells

Guicai Li[1,2*&], Xueying Zhao[1,2], Luzhong Zhang[1,2,], Jian Yang[1,2],

Wenguo Cui[3], Yumin Yang[1,2,*], Hongbo Zhang[3,4,5,*]

[1]Key laboratory of Neuroregeneration of Jiangsu and Ministry of Education, Nantong University, 226001, Nantong, P.R. China

[2]Co-innovation Center of Neuroregeneration, Nantong University, 226001, Nantong, P.R. China

[3]Shanghai Institute of Traumatology and Orthopaedics, Shanghai Key Laboratory for Prevention and Treatment of Bone and Joint Diseases, Ruijin Hospital, Shanghai Jiao TongUniversity School of Medicine, 197 Ruijin 2nd Road, Shanghai 200025, PR China

[4]Pharmaceutical Science Laboratory, Åbo Akademi University, 20520, Turku, Finland

[5]Turku Bioscience Centre, University of Turku and Åbo Akademi University, 20520, Turku, Finland

Corresponding Author: Tel: +358 2 215 4141;

E-mail address: gcli1981@ntu.edu.cn(Guicai Li)

yangym@ntu.edu.cn(Yumin Yang)

hongbo.zhang@abo.fi (Hongbo Zhang)

Abstract:

Peripheral nerve regeneration is a clinical challenge that tremendously affected the patients' quality of life. Recently, anisotropic microtopology has shown promise in treating peripheral nerve regeneration. However, the systematically investigation of how micropatterning influence Schwann cells (SCs), including morphology, biofunction and gene expression etc, has never been investigated. Herein, we fabricated the chitosan micropatterning with four different ridge/groove (RG) and subsequently cultured the SCs on those samples. As a result, the SCs showed obvious orientationally growth to micropatterning and 30/30 μm size showed the best regulation effect. And in the meantime, 30/30 μm size did not affect the DNA synthesis phase of SC cells (G2 and S phase) and significantly down-regulated both the relative protein level of N-cadherin and β-catenin from SCs. More importantly, the anisotropic micropatterning could significantly up-regulate the expression of several key genes of SCs related to neuronal plasticity and axon regeneration (smad6), cytoskeleton development (β -actin) and myelination (MPZ). Overall, the results demonstrated that the anisotropic chitosan micropatterning with 30/30 μm size can regulate SCs' orientation well with a tendency to myelination; and the systemic evaluation provide mechanical understanding, which acts as important references for future design of anisotropic biomaterials for peripheral nerve regeneration.

Keywords： peripheral nerve; chitosan; anisotropic microtopography; Schwann cell; physiological function.

1 Introduction

Peripheral nerve injury (PNI) has been a serious problem with negative influence on people's life and health[1, 2]. The nerve conduits fabricated by various biomaterials have been the most commonly clinical used method for repairing the damaged peripheral nerve[3]. However, its effect is unsatisfied in clinical request in comparing to autologous grafts, which may be ascribed to several factors, including diversely physical, chemical and biological cues. In the last two decades, more and more researches have focused on investigating the effect of surface properties (elasticity, topology, charges, etc) on tissue reconstruction and regeneration[4, 5]. The micropatterning technique, as a method for producing specific surface topology, has been widely used to fabricate various anisotropic and isotropic topological structures (e.g. grooves, pillars, columns, etc) with different sizes for better mimicking the naturally physiological structure of tissues[6]. Pati, et al[7] fabricated decellularized extracellular matrix (dECM) micropatterning with embedded cells via bioprinting method, which could simulate an optimized microenvironment for the growth of three-dimensional tissue. The constructs with high cell viability and functionality were proven to have potential application in adipose, cartilage and heart tissues. The micropatterned polymeric films including polystyrene (PS) and poly(lacticacid) (PLA) were found to affect the morphology, alignment and trans-differentiation of bone marrow-derived rat mesenchymal stem cells (MSCs) towards Schwann cell (SC)[8]. In addition, other micropatterned scaffolds including polydimethylsiloxane (PDMS)[9], polycaprolactone (PCL) [10], collagen[11] and chitosan[12] were all proven to be

beneficial for nerve regeneration. However, most studies just focused on the morphology regulation of cells by anisotropic microtopology, while it is more important to understand the influence of anisotropic microstructure on intracellular variation cells, such as cell cycle, expression of gene and protein, etc.

Until now, Schwann cells have been widely used as the model cells in peripheral nerve regeneration, because Schwann cells can form myelin sheath and promote axon growth of peripheral nerve by secreting trophic support molecules and establishing supportive growth matrix [13]. Moreover, the orientation of Schwann cell plays a pivotal role in guiding regenerating axons[14]. Hsu et al, found that the microgrooved silicon wafer with different size could effectively regulate the orientation of Schwann cells, and the cell alignment guided by surface microgrooves was found to be time dependent [15]. The oriented growth of Schwann cells induced by anisotropic micropattern was beneficial for their migration[16], which could then further precede neurite outgrowth during nerve regeneration[17]. In another study, Schwann cells were found to direct peripheral nerve regeneration through the netrin-1 receptors, deleted in colorectal cancer (DCC) and uncoordinated (Unc) 5H2. These findings demonstrated that Schwann cells could promote or hinder axon outgrowth via DCC and Unc5H2 signaling, thus providing an important mechanism on how Schwann cells regulate nerve regeneration[18]. In addition, in our previous study, the orientation of Schwann cells could be well regulated by the anisotropic chitosan micropatterning, which was also further found to be beneficial for accelerating nerve regeneration via *in vivo* rat experiment[4, 19]. Thus, rationally regulating the orientation growth of SCs

will be beneficial for peripheral nerve regeneration. Nevertheless, as mentioned above, it is facile to adjust SCs alignment via anisotropic micropatterning, while the detailed effect of anisotropic micropatterning on Schwann cells skeleton arrangement, cycle, gene and protein expression related to myelination is still unclear. It will be critical to understand the underlying mechanism in order to support the designing of new nerve grafts.

Thus, in the present study, the anisotropic ridge/groove structured chitosan micropatterning with four different sizes were fabricated by micromolding method in order to further reveal the mechanism of chitosan micropatterning on the physiological function of SCs. The morphology and stability of chitosan micropatterning were characterized. The attachment, proliferation, and morphological indexes of SCs were evaluated. And the cell cycle, protein and gene expression related to myelination of SCs were critically analyzed. Finally, the relationship between the anisotropic chitosan micropatterning and Schwann cells physiological function was discussed. It is anticipated that the study wound provide further understanding on the effect of anisotropic microstructure on Schwann cells' biofunction for nerve regeneration.

2 Materials and methods

2.1 Fabrication and characterization of anisotropic chitosan micropatterning

Firstly, the PDMS stamps (Dow Corning, USA) were prepared according to our previous study[4], and four sizes of ridge/groove were selected, i.e. 10/10, 20/20, 30/30, and 50/50μm. The anisotropic chitosan micropatterning was also prepared in terms of

our previous study[4]. In brief, a 100 μL of 1% chitosan (deacetylation degree: 92.3%, Nantong Water Products Institute, Jiangsu, China,) solution was added onto round glass coverslips (diameter: 10 mm, Feiao, Co.Ltd, China). Then, the PDMS stamps were used to press on the coverslips and kept at room temperature for at least 48 h. Thereafter, the PDMS stamps were peeled off and the chitosan micropatterning was left on coverslips. Finally, the chitosan micropatterning was rinsed with 1 M NaOH and dried before use. The chitosan coating without micropatterning was used as control. After coating with a gold layer (~50 nm thickness), the prepared anisotropic chitosan micropatterning was observed by a scanning electron microscope (SEM, Hitachi S-3400 NII, Japan) at a vacuum degree of 1.33×10^{-4} Pa with the acceleration voltage of 20 kV. The water contact angle of the prepared samples was measured using a contact angle measurement instrument (JY-PHa, Chengde), three parallel samples were used for each measurement.

The stability of the prepared anisotropic chitosan micropatterning was evaluated as following: the coverslips with anisotropic chitosan micropatterning were immersed into phosphate buffer saline (PBS, pH 7, Hyclone) for different periods (1, 3, 5, 10, 20 and 30 d). Then, at each time point, the samples were taken out and completely dried. Finally, all the anisotropic chitosan micropatternings were observed under an optical microscope (OM, Leica, Germany).

2.2 Schwann cells culture and evaluation

Schwann cells from lumbar dorsal root and sciatic nerves of Sprague-Dawley rats (SD, born 1-3 d old) were harvested and culture in Dulbecco's modified Eagle's medium

(DMEM, Invitrogen, CA) containing 10% fetal bovine serum (FBS, Sigma-Aldrich, USA) as described previously[12]. Then, Schwann cells with concentration of 5 $\times 10^4$ cells/mL medium were cultured on the sterile samples in 24-well plate separately for 1, 3 and 5 days after purification.

For the attachment and proliferation test of Schwann cells on different samples, at each time point, i.e. 1, 3 and 5 days , the DMEM medium was first discarded and the samples were thoroughly rinsed with PBS for three times. And then 500 μL of 10% cell counting kit 8 reagent (CCK-8, BD Biosciences, San Jose, CA) was added to the wells and incubated at 37 ℃ for 4 h. Subsequently, 150 μL of the supernatant in each well was extracted and added to a 96-well plate. Finally, a micro-plate reader was used to obtain the optical density at 450 nm.

For the morphology observation of Schwann cells on different samples, the samples at each time point were firstly rinsed with PBS for three times, and then fixed with 4% paraformaldehyde (Feiao, Co. Ltd, China) for at least 2 h. Subsequently, 100 μL of 1% toluidine blue (TBO, Sigma-Aldrich) solution was added onto the samples and incubated for 30 min at room temperature. Thereafter, the samples were thoroughly washed with PBS for five times and observed under an optical microscope. For each sample under the same magnification, five to seven fields were selected in order to obtain the statistical significance. Three parallel samples were used in the above tests.

2.3 Time-lapse video analysis

The initial attachment and moving track of Schwann cells were analyzed by a Time-

lapse video captured with an inverted time-lapse Olympus X181 Cell-R microscope, which was equipped with 960 or 9100 objective lenses and a Hamamatsu CCD ORCA/AG camera. The cells were first cultured on the samples with a concentration of 5×10^4 cells/mL and incubated for 4 h of adherence. And the samples were rinsed gently and transferred to a measurement chamber with humid environment of 37 ℃, 5% CO_2. Then, the movement of Schwann cells were captured every 5 min for 24 h. The images were processed and analyzed with Cell-R software (Olympus, Japan) and Image Pro Plus software. For the moving track of Schwann cells, the x/y coordinates of cell nuclei from each video were recorded for five cells/per field with intervals of 10 min. The original data were normalized to a common point. The cumulative value was obtained by calculating the totally traveled distance of Schwann cells regardless of the direction of movement

2.4 Morphological index of Schwann Cells

The morphological indexes, including spreading area, orientation angle (OA) and the ratio of lateral axis/vertical axis, of SCs were measured for further evaluating the effect of anisotropic chitosan micropatterning on Schwann cells morphology as reported by Li et al [12, 20]. The OA and the ratio of lateral axis/vertical axis of SCs on all different samples was calculated using Image Tool software (UTHSCSA, Version 2.0) by importing TBO staining images of Schwann Cells. Generally, the small OA and ratio of lateral axis/vertical axis indicates a prolonged cell body, i.e. an obvious elongation alignment of cells. For each sample, seven random sight fields were chosen to observe, and ten cells in each sight field were analyzed. Three parallel samples were used for

each micropattern size in order to obtain a statistical assessment.

2.5 Cell cycle analysis by flow cytometry

The distribution of Schwann cells in the different phases was determined using a flow cytometry (BD Bioscience, San Jose, CA). After culture on anisotropic chitosan micropatterning and control samples for 5 d, Schwann cells were digested and centrifuged at 1000 rpm for 10 min. Afterwards cells were gently re-suspended in 50 mg/mL hypotonic propidium iodide (PI) solution (diluted in 0.1% sodium citrate and 0.1% TritonX-100, Sigma-Aldrich), and subsequently incubated in dark at 4 ℃ for at least 30 min. Thereafter, the cells were analyzed by a flow cytometry. The measurement should be finished during 1 h period.

2.6 Western blot analysis

Schwann cells were cultured on different samples for 5 days, then the cells were rinsed with PBS for three times and treated with lysis buffer containing protease inhibitors (1:100) on ice for 15 min. (Promega, Madison, WI). Thereafter, cells were scratched with a scraper and transferred to a centrifugal tube (1.5 mL). After centrifugation at 14,000 g for 15 min, the supernatant was collected to obtain the total protein concentration by BCA-protein assay method (Biyuntian, China). The protein concentration was adjusted to the same loads. Subsequently, the protein expression levels of N-cadherin and β-catenin was determined by western blot analysis as described previously [21]. The primary antibodies were polyclonal antibody rabbit anti-N-cadherin (1:2000 dilution, Abcam) and polyclonal antibody rabbit anti-β-catenin

(1:1000 dilution, Abcam). The secondary antibody was horse radish peroxidase (HRP)-conjugated goat anti-rabbit IgG (1:1000dilution). The immunoreactive bands were scanned by enhanced chemiluminescence (LICOR, Lincoln, NE) and analyzed with PDQuest 7.2.0 software (Bio-Rad). The β-actin (1:1000) was served as an internal control.

2.7 Gene expression

The differential gene expression was analyzed by a professional Novel Gene Analysis Company (Shanhai, China). In brief, firstly, the total RNA of Schwann cells was extracted using TRIzol reagent (Invitrogen, USA) according to the manufacturer's protocol and stored at −80 °C. Then, the RNA with RNA integrity number (RIN) larger than seven was used to construct cDNA library. The pure messenger RNA (mRNA) could be obtained using a Dynabeads mRNA Purification Kit (Epicentre Technologies). The cDNA library was prepared via an Ion Total RNA-Seq Kit v2 (Epicentre Technologies) and processed for proton sequencing according to commercially available protocols. The reads per kilobase per million (RPKM) method was used to measure the expression level for each gene [22]. The heatmap was obtained by MapSplice[23, 24]. And finally the the EB-Seq algorithm was used to evaluate the differential gene expression on both micropatterned and unmicropatterned samples.

2.8 Quantitative real time RT-PCR

The RNeasy Mini Kit (Qiagen, Valencia, CA, USA) was used to isolate total RNA from Schwann cells in terms of the manufacturer's protocol followed by the treatment of

DNA-Free RNAKit (Zymo, Irvine, CA, USA). Then, the reverse transcription was performed using 2 mg of total RNA, Superscript III (Life Technologies) and anchored oligo-dT primers (Operon, Huntsville, AL, USA). The software Oligo Explorer 1.2 (Genelink, Hawthorne, NY, USA) was used to design specific primers for target genes (Table.1). GAPDH as an endogenous control was used for normalization of expression levels. An ABI7500 instrument (Applied Biosystems, Foster City, CA, USA) was used to perform the real-time RT-PCR reactions. The parameters for amplification reactions were set as follows: 2 min at 50℃, 10 min at 95℃, and 40 cycles of 95℃ for 15 s and 55℃ for 30 s, and 68℃ for 30 s. The comparative Ct method was used to quantify the fold variation in gene expression by means of 2−(Ct treatment−Ct control). The comparison was based on the target gene expression (normalized to the endogenous control GAPDH) of Schwann cells between the micropatterned samples and the flat surface.

2.9 Patch Clamp

Firstly, Schwann cells were cultured on samples for 5 days, then the medium was trashed and cells were rinsed with PBS for five times. After that, a 1wt.% papain was added and incubated for 3 mins. Then, patch clamp recordings with PatchMaster software were performed using a double patch clamp setup (EPC10, Heka Elektronik, Lambrecht/Pfalz, Germany) in current clamp mode. Borosilicate glass patch pipettes with a resistance of 3-4 MOhm were pulled using a micropipette puller (Model P-97, Sutter Instrument Company). The manipulation of patch clamp was monitored under microscopic control (IX 50, Olympus) using a stepper motor based micromanipulator

unit (Mini 25, Luigs and Neumann). For current clamp recordings, the membrane current was set to zero. The automated step protocol with the +5-mV steps protocol was used to characterize the voltage-gated ion channels. Action potentials were induced with 60 ms, +100-pA square-shaped pulses. The peak resistance was 1000~1200 MOhm, and membrane resistance was 7 MOhm. The intracellular solution contained 5mM KCl, 0.5mM $CaCl_2$, 140mM NaCl, 5.5 mM potassium-D-gluconate, 5mM EGTA, 0.5mM $MgCl_2$, 2mM K_2-ATP and 10mM HEPES at pH 7.2. The external bath solution contained 3mM $CaCl_2$, 0.1mM $MgCl_2$, 137mM NaCl, 5mM KCl, 0.01mM glycine, 10mM glucose, and 5mM HEPES at pH 7.2. All experiments were performed at room temperature (25 °C).

2.10 Statistical analysis

The analysis of variance was used to calculate the significant differences between groups. A one-way ANOVA test was used for statistics by SPSS software (Chicago, USA). All the results are reported as the mean±SD of three independent experiments. $P < 0.05$ was considered statistically significant.

3 Results

3.1 Morphology and stability of anisotropic chitosan micropatterning

The morphology and water contact angle of the prepared anisotropic chitosan micropatterning is shown in Fig.1a. Obviously, a clear ridge/groove structure was seen on the surface of all micropatterned samples. The ridge and groove were both intact without crack, the width of ridge or groove increased with the micropatterning size.

While, no micropatterning structure was found on the control sample surface. In addition, it was found that the water contact angle of sample with width of 10/10 μm was 58.54 ± 2.21°, which was the largest among all the samples, while the control sample without micropatterning structure possessed the smallest water contact angle of 24.77 ± 1.01°, indicating the enhanced surface hydrophobicity through micropatterning. For all the micropatterned samples, an obvious decreased water contact angle with increasing micropatterning size was observed, suggesting the possible influence of ridge/groove width on surface wettability. Thereafter, the stability of all prepared samples was evaluated by PBS immersion for various periods. Fig.1b displays that the chitosan micropatterning remained clear and kept the complete stripe structure with the prolonged immersion days, and no erosion phenomenon was detected for any of the samples, which indicated the very good stability of the micropatterned chitosan film. The results above demonstrated that the chitosan micropatterning with clear ridge/groove structure and good stability could be successfully fabricated using micromolding method on coverslip surface. The width of ridge/groove could affect the surface wettability of anisotropic chitosan micropatterning.

3.2 Time-lapse video

The movements of Schwann cells on samples with or without micropatterning structure were firstly compared using a time-lapse video. Obviously, Fig. 2 displayed that the cell morphology as well as cell spreading was conspicuously different on all the samples. On the 10/10 μm sample, some cells could lie across several ridges and groove due to the smaller patterning size than cell body. The cell soma was stretched and cells

elongated along one direction before contracting to a spherical shape, but some other cells formed clusters. Notably, the cell alignment had clear deviation with the micropatterning structure and most cells moved randomly without orientation as indicated by the track curve (Fig.2F). In contrast, Schwann cells on three other micropatterned samples displayed stretchable shape with alignment growth with the micropatterning structure, suggesting much better regulation on orientationally cell growth. Interestingly, cells continually contracted and extended their lamellipodia for movement. The track curve (Fig.2G-I) of cell movements further indicated that most cells possessed an orientationally growth with the patterning on the 20/20 μm, 30/30 μm and 50/50 μm samples, except that individual cell outgrowing was detected on the 50/50 μm sample due to the too large patterning size. However, as compared to cells on the micropatterned samples, Schwann cells on the control sample only displayed round shape initially and formed clusters lastly. And Fig.2J further indicated that the cells on control sample displayed irregular movement with randomly directional changes. In addition, it should be mentioned that the horizontal migration distance of Schwann cells on all micropatterned samples (>1.6mm) were significantly larger than that on the control samples (<0.7mm), while cells on control sample had the largest vertical migration distance compared with other samples, confirming that the anisotropic structure could obviously promote Schwann cells migration, which will be beneficial for accelerating nerve regeneration.

3.3 Observation of cell morphology

The morphology of Schwann cells was observed by OM via TBO staining after

culturing for 1, 3 and 5 days, respectively. Fig.3a shows that Schwann cells on 10/10 μm sample had directional growth at the 1st and 3rd day of culture, a random spreading morphology without alignment behavior was observed at the 5th day of culture. Moreover, Schwann cells were found to have the trend of going across the ridge/groove structure of 10/10 μm during the culture period. However, cells on the samples with RG size of 20/20, 30/30 and 50/50 μm displayed better alignment growth than that on 10/10 μm at different time points. It was seen clearly that the cells proliferated on the surface of the samples with increasing culture time, and the connection among cells was established, which was more obvious for cells on the 30/30 μm sample at the 3rd day of culture. Then a cell sheet was formed after further culture for 5 days. More importantly, Schwann cells on 30/30 μm sample kept well orientationally growth and exhibited a manifest proliferation from the 1st day to the 5th day of culture compared with other anisotropic chitosan micropatterning. However, the connection of cells on 50/50 μm samples was relatively weak even after culturing for 5 days, and most cells displayed a single orientation growth along with the micropatterning structure. In contrast, Schwann cells on the control sample displayed random distribution without any alignment growth. In addition, both the 20/20 μm and 30/30 μm samples displayed more obvious cell proliferation at the 5th day of culture compared to 10/10 μm and 50/50 μm samples, indicating the micropattern with suitable width may be beneficial for cell proliferation.

For further observing the cytoskeleton distribution of Schwann cells, the cytoskeleton and nucleus were stained by phalloidin and DAPI fluorescence dye at the 5th day of

culture, respectively. Fig.3b displays that Schwann cells on 30/30 μm samples showed the most obvious orientationally growth compared with other samples. Schwann cells grew along with the microgroove direction, and the typical cell growth of end-to-end was observed on the 30/30 μm sample. Moreover, a cell sheet was further obtained at the 5th day of culture. However, for 50/50 μm sample, cells' orientation was different as other micropatterned samples. Some cells grew with random direction in the micropatterning structure as indicated by the arrows. In addition, cells on 10/10 μm and control samples were found to distribute randomly without orientationally growth.

3.4 Morphological index analysis

Morphological index, including spreading area, OA and the ratio of lateral axis/vertical axis, reflects the effect of micropatterning on the morphology development of Schwann cells. Fig.4A shows that no obvious difference of spreading area of Schwann cells was detected on the same sample surface after culturing for various culture periods ($P>0.05$), but the spreading area of cells on different samples was distinct from each other. Obviously, Schwann cells on 30/30 μm sample displayed a much smaller spreading area than that on the samples of 10/10, 20/20, 50/50 μm, and control samples ($P<0.05$). Interestingly, the spreading area of Schwann cells firstly decreased with the increasing micropatterning size from 10 to 30 μm, while then increased when the micropatterning size was 50 μm. The micropatterning structure with a suitable size could regulate cell spreading. The OA of Schwann cells on different micropatterning was evaluated after culturing for 1, 3 and 5 days, respectively (Fig. 4B). For cells on 20/20 μm, 30/30 μm and 50/50 μm samples, the OA was much smaller than

that on 10/10 μm sample ($P<0.05$) at the same time point, indicating a better orientationally cell growth on the former three samples, especially for the 30/30 μm and 50/50 μm samples. In addition, it was noted that the OA of cells on 10/10 μm sample showed no obvious variation during the whole culture periods, whereas cells on 20/20 μm sample displayed an obviously increased OA from the 1st day to the 5th day of culture. However, for the 50/50 μm sample, the change of cells' OA was not as obvious as that on 20/20 μm sample though a little increase was observed. In contrast, Schwann cells on 30/30 μm samples exhibited an obvious OA decrease with the increasing culture periods, indicating the better alignment growth of cells for longer time. Otherwise, the OA of cells on flat sample was not analyzed here since there was no orientation distribution of Schwann cells on the control samples.The ratio of lateral axis/vertical axis of Schwann cells after culture for different periods was presented. As shown in Fig. 4C, cells on 10/10 μm sample and control sample had the similar ratio of lateral axis/vertical axis, and there was no obvious difference during the whole culture periods ($P>0.05$). While, notably, the cells on 20/20 μm, 30/30 μm and 50/50 μm samples showed smaller ratio of lateral axis/vertical axis than that on 10/10 μm sample and control sample, but no significant difference was found between 20/20 μm and 30/30 μm samples, indicating good alignment growth of the Schwann cells.

3.5 Cell cycle

Cell cycle studies could reflect the dynamic balance of physiological activities such as cell proliferation, differentiation and apoptosis. For better understanding whether the anisotropic micropatterning structure wound affect cell activities, the cycle of Schwann

cells cultured on various samples for 5 days was measured using flow cytometer. As shown in Fig.5, Schwann cells on 10/10 μm, 20/20 μm, 30/30 μm, 50/50 μm samples displayed a bit higher population (80.6%, 81.58%, 78.49% and 80.75%) of cells at phase G1, which indicate the DNA pre-synthesis phase and cell proliferation initiation, than the control sample (77.67%), however the difference between 30/30 μm and control samples was neglectable. And, the percentage of cells at phase G2, which suggested the consistent post-synthesis phase of DNA, was similar among all samples. In addition, Schwann cells on control samples showed the largest cell population (9.59%) in phase S compared with 10/10 μm, 20/20 μm, 30/30 μm, 50/50 μm samples (6.4%, 5.9%, 7.9%, 5.94%), indicating that more cells in control samples were at DNA active synthesis phase. And again, the difference between 30/30 cm to control sample was the smallest, indicating that 30/30 μm size had minimum affect on the cell cycle. The above results demonstrated that though the DNA synthesis of Schwann cells was a bit affected by anisotropic microstructure, this effect was very minor and suitable micropattern size could further reduce the effect.

3.6 Western blot analysis

The N-cadherin and β -catenin complexes are located at the cell-substrate interface within the lamellipodium in radial structures. β -catenin is a complex adaptor protein related to tension-dependent conformational change. Besides, β -catenin could alternate actin networks during cell-cell contact via cadherin-catenin complexes[25]. Thus, the protein expression of N-cadherin and β-catenin from Schwann cells were further analysed by western blot method after 5 days of culture. Fig.6A exhibited that

the expression of N-cadherin was significantly higher in Schwann cells on 10/10 μm and 20/20 μm samples than that on other samples (*P<0.05). Schwann cells on the control samples displayed the lowest expression of N-cadherin compare with all the micropatterned samples. It was seen clearly that the expression of N-cadherin decreased with the ascending anisotropic micropatterning size. For the expression of β-catenin, the similar trends in all micropatterned samples were obtained except for the control samples, with the highest expression of β-catenin. The electrophoresis bands in Fig.6B further verified the above results.

3.7 Gene expression profiling of miRNAs and pathway analysis

As based on the above experimental results, SCs on 30/30 μm sample possessed the best alignment growth and proliferation compared with other micropatterned samples. Therefore, to examine the miRNA expression change in SCs grown on anisotropic micropatterning, the miRNA expression profiles in SCs that grown on 30/30 μm and on control samples for 5 days, were studied using high-throughput transcriptome RNA sequencing (RNA-Seq). Fig.7A exhibited that a total of 11 miRNAs in cells showed dynamic up-regulation and those miRNAs were related to cell adhesion, cell endocrine, cell motility, and axon guidance. While 17 miRNAs were down-regulation, and it was found that those miRNAs mainly referred to apoptosis, inflammation, cytoskeleton and cell differentiation (Fig.7C). Further on, the pathway enrichment analysis (Fig.7B) was performed, and it was found that the anisotropic micropatterning with 30/30 μm size mainly activate four important signal pathways, including TGF-β, cell adhesion molecules (CAMs), thyroid hormone synthesis and salivary secretion, which are critical

for cell growth, development, metabolism and endocrine[26]. Further study needs to be carried out to verify these signal pathways.

3.8 QRT-PCR analysis

The SCs on 30/30 μm sample after 5 days of culture with observed phenotypic or morphological changes were further corroborated by gene expression using QRT-PCR analysis. And the SCs on flat control sample were used as comparison. The mRNA levels of SC specific markers such as β-actin, MBP, MPZ, S100, SMAD6, and Sox10 were monitored, while GAPDH served as the internal control. RT-PCR analysis in Fig.8 displayed the gene expression difference of specific markers for SCs grown on anisotropic chitosan micropatterning with various sizes, in comparison to the flat control on day 5. The gene expression of MPZ, S100, SMAD6 and β-actin by SCs on all anisotropic chitosan micropatterning were all significantly higher ($P<0.05$) than that by cells on flat control. However, there was no obvious difference for the gene expression of MBP and Sox10 by SCs between the micropatterned chitosan and flat control samples ($P>0.05$).

3.9 Investigation of Schwann cells by patch clamp measurement

To further penetrate the influence of anisotropic micropatterning effect on membrane potential change of Schwann cells, we therefore investigated the potential variation of cell membrane on flat and micropatterned chitosan via patch clamp measurements. Cell was patched in the current clamp mode, and a typical recording of potential variation of Schwann cells is shown in Fig. 9. Schwann cells without alignment growth (CTL) displayed a potential of around -20 mV, however, cells with obvious orientation growth

(30/30) on micropatterned samples showed a potential of around -15 mV. The difference of potential variation of cells with or without alignment morphology was significant ($P<0.05$). The results indicated that anisotropic micropatterning structure could change the membrane potential of Schwann cells, thus may further cause reaction in the intracellular, such as protein and gene difference, and pathway activation.

4 Discussion

PNI is still a world-wide nerve system disease, which seriously affect the health and life of the patients[1, 27]. Autologous graft is the golden standard for repairing PNI but limited to the size mismatch, source limitation, and permanent damage to the donor site[28]. The artificial nerve implants made from various biomaterials have been used for peripheral nerve regeneration in the last several decades[29]. Among which, chitosan as natural biomaterials has been widely applied in different tissue engineering fields including nerve, skin and tendon, etc[30]. However, the single chitosan scaffolds in per se were not enough to repair the damaged nerve, especially for the long-distance gap. Thus, the effect of single chitosan implants was still not as good as the autologous grafts and should be further enhanced. It has been well known that the surface topography of biomaterials play an important role in regulating tissue regeneration. We also found that the anisotropic chitosan micropatterning could well regulate orientation growth and skeleton re-arrangement of Schwann cells[4]. However, the effect of anisotropic chitosan micropatterning on the physiological function of cells including cell cycle, gene expression and related mechanism was still not clear. Therefore, in the present study, the anisotropic chitosan micropattening with four ridge/groove sizes was

further fabricated, and the effect on morphology, cell cycle, gene and protein expression of Schwann cells was investigated. The underlying mechanism of chitosan micropatterning on Schwann cells was also penetrated.

The integrity of the micropattening structure is the key step for the sequential study of cell behavior. Thus, the basic properties of the chitosan micropatterning including morphology, wettability, and stability are firstly investigated. As shown by SEM, the chitosan micropatterning with integral and clear ridge/groove structure could be well fabricated using micromolding method, which is consistent well with our previous study[4]. Only the integral micropatterning structure could well regulate the alignment growth of cells. Or else, the incomplete microstructure may lead to the outgrowth of the neurites and result in experimental fakes. The wettability is important for cell attachment and proliferation, since a suitable hydrophobic or hydrophilic surface could induce the formation of focus adhesion of cells and further influence their migration. Interestingly, the hydrophobicity is decreased with the ascending micropatterning size, which may be called a ‘lotus-like’ effect[31], because the water droplet may lie across several ridges without contacting the groove bottom due to the surface tensile effect when the micropatterning size is too small. However, with the increasing of patterning size, the water droplets may contact with the groove bottom and form capillary interaction, thus the droplet spreads and hydrophilicity is enhanced. Additionally, the stability of the chitosan micropatterning would be beneficial for the performance of implants, especially for long term implantation[32]. After immersion in PBS for up to 30 days, our prepared anisotropic chitosan micropatterning was shown to be very stable

without obvious degradation. Therefore, the good stability may pave the way for the orientation growth of Schwann cells and nerve regeneration for long term implantation.

Schwann cells associated with axon regeneration and function are the key glial cells in peripheral nerve system, which could elongate and form myelination wrapping the axon and secret various neurotrophic factors for promoting axon growth[33]. After PNI, Schwann cells at the site of distal and proximal stump will undergo several changes for axon outgrowth, including dedifferentiation, loss of myelination phenotype, formation of basal lamina for axon regrowth[34]. Schwann cell movement in real time was firstly monitored using Time-lapse video. The anisotropic chitosan micropatterning could not only induce alignment growth but also promote migration of Schwann cells compared with flat control, while the rapid migration of Schwann cells will provide key platform for axon regeneration of neuron[35]. Thus, it is reasonable to believe that the anisotropic micropatterning may accelerate nerve regeneration after implantation. The morphological evolution of cells could affect their growth and biological function[36], therefore, we then evaluated the effect of anisotropic chitosan micropatterning on Schwann cell morphology variation. The results of immunofluorescence staining and morphological indexes showed that for the smaller size (10μm) less than the cell size in per se, cells could lie across several ridges or grooves. Thus, the regulation effect of cells orientation was not obvious, and most cells on small micropatterning size displayed random direction. However, when the micropatterning size increased and approached to the cell size (20 ~ 30μm), an obvious alignment growth of cells was obtained, especially for the ridge/groove size with 30/30 μm. The results further

indicated that the cell morphology could be well regulated when the micropatterning size was approaching to the cell size, which was consistent well with previous report by Hsu, et al[15]. In addition, interestingly, we found an obvious proliferation of Schwann cells on micropatterns with ridge/groove size of 20/20 μm and 30/30 μm, while not on 10/10 μm and 50/50 μm. Unadkat, et al. also reported that a certain spatial distribution could influence cell proliferation[37]. A similar results were further confirmed by Hohmann, et al., who found that the 25 μm spaced posts showed a significantly higher proliferation of SaOs-2 cells than 10, 40 and 50 μm [38], though the pattern structure and composition were different. Furthermore, He, et al reported that the topographies may initiate Hedgehog-Gli1 signaling and then influence endothelial cells proliferation[39]. However, the underlying mechanism of anisotropic chitosan micropattern on Schwann cell proliferation was still needed to be penetrated.

Besides morphology, the normal biological function of Schwann cells, such as DNA synthesis, is directly related to the proliferation and differentiation of cells[40], as DNA could influence the development and information transduction. Thus, we evaluated the effect of anisotropic micropatterning on cell cycle. Obviously, 30/30 μm size could enhanced the synthesis phase compared with other sizes, indicating the anisotropic micropatterning could activate a more vigorous DNA synthesis. Since miRNAs have been found to regulate the myelination of Schwann cells [41], and the miRNAs expression initiated by PNI could mediate multiple cellular events by activing or suppressing related target genes[42]. Thus, the expression profile of miRNA in Schwann cells stimulated by anisotropic chitosan micropatterning (30/30 μm) was

studied using RNA-Seq technique. Here, 28 miRNAs with up- or down- regulation expression were obtained for the first time. After referring to the GeneCards (https://www.genecards.org/), the anisotropic micropatterning mainly upregulated genes referring to cell adhesion (Hoxb6, Ncan), cell endocrine (Rn5-8s), cell motility (Atp2b4, Vcan), and axon guidance (Dpys13), while downregulated genes referring to apoptosis (Apopt1, Hspa9), inflammation (Mif, Anxal), cytoskeleton (Map4, Atp1b1, Tbcb) and cell differentiation (Ntrk3, Itga7). Thus, the results demonstrated that the anisotropic micropatterning could not only affect cell morphology but also intracellular genes. Here, we initially confirmed the up- or down- regulated genes using RNA-Seq technique. Next step, more work will be done to further figure out the relationships between anisotropic micropatterning and above genes by signal pathway analysis and gene knockout technique, etc. In particular, the expression levels of SC specific markers such as MBP, MPZ, β-actin, S100, SMAD6, and Sox10 were monitored. Notably, anisotropic chitosan micropatterning (30/30 μm) could obviously up-regulate several key specific markers of SCs including β-actin, MPZ, S100 and SMAD6. β-actin is the main genes related to cell skeleton[43], the up-regulation of the gene demonstrates that the ridge/groove structure could remold the skeleton arrangement of Schwann cells. As one of the axonal membrane proteins, the up-regulation of SMAD6 has been reported to reflect the neuronal plasticity and axon regeneration process [44]. In the present study, an obvious up-regulation of SMAD6 in SCs on chitosan micropatterning was anticipated to promoting axon regeneration better than that on flat control. Interestingly, the 30/30 μm size also significantly increased S100 expression compared to flat control

($P<0.05$). S100 has been found to be related to axon diameter and myelination[45], thus the huge up-regulation of S100 illustrated that the micropatterning may effectively regulate the axon outgrowth and myelination process, and thus may be helpful for nerve regeneration. As mentioned above, the anisotropic chitosan micropatterning could cause skeleton re-arrangement, which may change the membrane potential of cells and affect sequential gene and protein expression[46]. Therefore, we then used patch clamp to study the membrane potential variation of Schwann cells with different morphology under static condition. Obviously, a significant lower membrane potential of cell with alignment shape was obtained compared to that with spreading shape, indicating the morphology change of cells is accompanying with membrane potential variation, while many kinds of proteins are embedded in cell membrane[47], thus the potential change may have close relationship with the intracellular reaction of cells, including protein expression, gene difference and pathway activation. To the best of our knowledge, this is the first time to study the influence of morphology on the membrane potential change of Schwann cells using patch clamp. It is also reasonable to believe that the penetration of the relationship between cell morphology and membrane potential change may be beneficial for unrevealing the mechanism referring to the geometry-cell behavior.

Overall, based on the aforementioned, it is reasonable to believe that the micropatterning structure developed in the present study may be beneficial for cytoskeleton rearrangement, axon outgrowth, myelination and neuronal plasticity, thus displaying potential promising for peripheral nerve regeneration. A possible reason may be that the anisotropic micropatterning cause skeleton variation of Schwann cells,

which then changes the membrane potential and subsequently activates the related signal pathway to up/down- regulate gene expression referring to various physiological function. However, for better revealing the underlying mechanism of anisotropic micropatterning effect on nerve regeneration, a further work referring to the in situ hybridization and gene knockout for verifying the related signal pathway need to be performed.

5 Conclusion

The anisotropic chitosan micropatterning with various ridge/groove sizes was successfully fabricated using micromoulding method. The morphology of Schwann cells could be significantly well regulated by chitosan micropatterning with 30/30 μm size without negatively influencing the normal biological function of DNA synthesis. Chitosan micropatterning mainly regulated the alignment growth of Schwann cells via down-regulating the expression level of N-cadherin and β-catenin. The anisotropic micropatterning could upregulate genes referring to cell adhesion, cell endocrine, cell motility, and axon guidance, while downregulate genes referring to apoptosis, inflammation, cytoskeleton and cell differentiation. Further, the intermediates of anisotropic chitosan micropatterning were able to potentiate the orientation, proliferation and differentiation of Schwann cells by changing the membrane potential and mediating the expression level of several key genes including MPZ, β-actin, S100 and SMAD6, which may be beneficial for accelerating nerve regeneration. Overall, the study defines a basic pathway for anisotropic chitosan micropatterning mediated the morphology, function and gene expression of Schwann cells, and may shed light on the

design and development of new generation of artificial implants for peripheral nerve regeneration and other tissue regeneration.

Acknowledgement

The authors gratefully acknowledge the financial support of the National Natural Science Foundation of China (31830028, 31771054), National Key Research and Development Program of China (2016YFC1101600, 2018YFC11056), Directive Project of Science and Technology Plan of Nantong City (2018), 226 High-level Talent Training Project (2nd level, 2018 II-182) of Nantong City, Qinglan Project of Jiangsu Province.

Data Availability Statement

The raw/processed data required to reproduce these findings cannot be shared at this time due to technical or time limitation.

References

[1] T. Gordon, G.H. Borschel. The use of the rat as a model for studying peripheral nerve regeneration and sprouting after complete and partial nerve injuries. Experimental neurology, 287 (2017)331-47.
[2] Zuhal Altunkaynak Berrin, Delibaş Burcu, Altun Gamze, G.D. Ömür. Melatonin and sciatic nerve injury repair: a current perspective. Journal of Neurorestoratology, 6 (2018)49-60.
[3] J.M. Oliveira, C.R. Carvalho, J.B. Costa, R.L. Reis. Advanced Natural-based Biomaterials To Tackle The Current Challenges In Peripheral Nerve Regeneration. Tissue Eng Pt A, 22 (2016)S106-S115.
[4] G.C. Li, X.Y. Zhao, L.Z. Zhang, C.P. Wang, Y.W. Shi, Y.M. Yang. Regulating Schwann Cells Growth by Chitosan Micropatterning for Peripheral Nerve Regeneration In Vitro. Macromolecular bioscience, 14 (2014)1067-75.
[5] Z.L. Yang, Y. Yang, L. Zhang, K.Q. Xiong, X.Y. Li, F. Zhang, et al. Mussel-inspired catalytic selenocystamine-dopamine coatings for long-term generation of therapeutic gas on cardiovascular stents. Biomaterials, 178 (2018)1-10.
[6] A. Parandakh, A. Anbarlou, M. Tafazzoli-Shadpour, A. Ardeshirylajimi, M.M. Khani. Substrate

topography interacts with substrate stiffness and culture time to regulate mechanical properties and smooth muscle differentiation of mesenchymal stem cells. Colloid Surface B, 173 (2019)194-201.
[7] F. Pati, J. Jang, D.H. Ha, S.W. Kim, J.W. Rhie, J.H. Shim, et al. Printing three-dimensional tissue analogues with decellularized extracellular matrix bioink. Nature communications, 5 (2014)3935-42.
[8] A.D. Sharma, S. Zbarska, E.M. Petersen, M.E. Marti, S.K. Mallapragada, D.S. Sakaguchi. Oriented growth and transdifferentiation of mesenchymal stem cells towards a Schwann cell fate on micropatterned substrates. Journal of bioscience and bioengineering, 121 (2016)325-35.
[9] F. Pan, M. Zhang, G.M. Wu, Y.K. Lai, B. Greber, H.R. Scholer, et al. Topographic effect on human induced pluripotent stem cells differentiation towards neuronal lineage. Biomaterials, 34 (2013)8131-9.
[10] E.M. Jeffries, Y.D. Wang. Biomimetic micropatterned multi-channel nerve guides by templated electrospinning. Biotechnol Bioeng, 109 (2012)1571-82.
[11] H. Fujimaki, K. Uchida, G. Inoue, M. Miyagi, N. Nemoto, T. Saku, et al. Oriented collagen tubes combined with basic fibroblast growth factor promote peripheral nerve regeneration in a 15mm sciatic nerve defect rat model. Journal of Biomedical Materials Research Part A, 105 (2017)8-14.
[12] G.C. Li, X.Y. Zhao, W.X. Zhao, L.Z. Zhang, C.P. Wang, M.R. Jiang, et al. Porous chitosan scaffolds with surface micropatterning and inner porosity and their effects on Schwann cells. Biomaterials, 35 (2014)8503-13.
[13] R.P. Bunge. The Role of the Schwann-Cell in Trophic Support and Regeneration. Journal of neurology, 242 (1994)S19-S21.
[14] M.R. Feneley, J.W. Fawcett, R.J. Keynes. The role of Schwann cells in the regeneration of peripheral nerve axons through muscle basal lamina grafts. Experimental neurology, 114 (1991)275-85.
[15] S.H. Hsu, C.Y. Chen, P.S. Lu, C.S. Lai, C.J. Chen. Oriented Schwann cell growth on microgrooved surfaces. Biotechnol Bioeng, 92 (2005)579-88.
[16] C. Liu, J. Kray, V. Toomajian, C. Chan. Schwann Cells Migration on Patterned Polydimethylsiloxane Microgrooved Surface. Tissue engineering Part C, Methods, 22 (2016)644-51.
[17] R.F. Valentini, P. Aebischer, S.R. Winn, P.M. Galletti. Collagen- and laminin-containing gels impede peripheral nerve regeneration through semipermeable nerve guidance channels. Experimental neurology, 98 (1987)350-6.
[18] C.A. Webber, K.J. Christie, C. Cheng, J.A. Martinez, B. Singh, V. Singh, et al. Schwann Cells Direct Peripheral Nerve Regeneration Through the Netrin-1 Receptors, DCC and Unc5H2. Glia, 59 (2011)1503-17.
[19] G.C. Li, C.B. Xue, H.K. Wang, X.M. Yang, Y.X. Zhao, L.Z. Zhang, et al. Spatially featured porous chitosan conduits with micropatterned inner wall and seamless sidewall for bridging peripheral nerve regeneration. Carbohydrate polymers, 194 (2018)225-35.
[20] J. Li, K. Zhang, P. Yang, W. Qin, G. Li, A. Zhao, et al. Human vascular endothelial cell morphology and functional cytokine secretion influenced by different size of HA micro-pattern on titanium substrate. Colloids and surfaces B, Biointerfaces, 110 (2013)199-207.
[21] Y. Gu, Y.W. Ji, Y.H. Zhao, Y. Liu, F. Ding, X.S. Gu, et al. The influence of substrate stiffness on the behavior and functions of Schwann cells in culture. Biomaterials, 33 (2012)6672-81.
[22] A. Mortazavi, B.A. Williams, K. Mccue, L. Schaeffer, B. Wold. Mapping and quantifying mammalian transcriptomes by RNA-Seq. Nat Methods, 5 (2008)621-8.
[23] S. Oh, J. Ha, K. Lee, S. Oh. DegoViz: An Interactive Visualization Tool for a Differentially Expressed Genes Heatmap and Gene Ontology Graph. Appl Sci-Basel, 7 (2017)543-57.

[24] K. Wang, D. Singh, Z. Zeng, S.J. Coleman, Y. Huang, G.L. Savich, et al. MapSplice: Accurate mapping of RNA-seq reads for splice junction discovery. Nucleic Acids Res, 38 (2010)e178-87.
[25] B. Ladoux, E. Anon, M. Lambert, A. Rabodzey, P. Hersen, A. Buguin, et al. Strength Dependence of Cadherin-Mediated Adhesions. Biophysical journal, 98 (2010)534-42.
[26] D.R. Warner, M.M. Pisano, R.M. Greene. Nuclear convergence of the TGF beta and cAMP signal transduction pathways in murine embryonic palate mesenchymal cells. Cell Signal, 15 (2003)235-42.
[27] R.J. Li, Z.G. Liu, Y.M. Pan, L. Chen, Z.X. Zhang, L.J. Lu. Peripheral Nerve Injuries Treatment: a Systematic Review. Cell biochemistry and biophysics, 68 (2014)449-54.
[28] F. May, A. Buchner, K. Matiasek, B. Schlenker, C. Stief, N. Weidner. Recovery of erectile function comparing autologous nerve grafts, unseeded conduits, Schwann-cell-seeded guidance tubes and GDNF-overexpressing Schwann cell grafts. Disease models & mechanisms, 9 (2016)1507-11.
[29] Y. Iijima, T. Ajiki, A. Murayama, K. Takeshita. Effect of Artificial Nerve Conduit Vascularization on Peripheral Nerve in a Necrotic Bed. Prs-Glob Open, 4 (2016)e665-75.
[30] F. Croisier, C. Jerome. Chitosan-based biomaterials for tissue engineering. Eur Polym J, 49 (2013)780-92.
[31] H.J. Wang, Z. Yang, J. Yu, Y.Z. Wu, W.J. Shao, T.T. Jiang, et al. Preparation of lotus-like hierarchical microstructures on zinc substrate and study of its wettability. Rsc Adv, 4 (2014)33730-8.
[32] D. Depan, J.S. Shah, R.D.K. Misra. Degradation mechanism and increased stability of chitosan-based hybrid scaffolds cross-linked with nanostructured carbon: Process-structure-functional property relationship. Polym Degrad Stabil, 98 (2013)2331-9.
[33] X.S. Gu, F. Ding, Y.M. Yang, J. Liu. Construction of tissue engineered nerve grafts and their application in peripheral nerve regeneration. Prog Neurobiol, 93 (2011)204-30.
[34] T.D. Glenn, W.S. Talbot. Signals regulating myelination in peripheral nerves and the Schwann cell response to injury. Curr Opin Neurobiol, 23 (2013)1041-8.
[35] L.F. Gumy, E.T.W. Bampton, A.M. Tolkovsky. Hyperglycaemia inhibits Schwann cell proliferation and migration and restricts regeneration of axons and Schwann cells from adult murine DRG. Molecular and Cellular Neuroscience, 37 (2008)298-311.
[36] K.J. Chalut, E.K. Paluch. The Actin Cortex: A Bridge between Cell Shape and Function. Dev Cell, 38 (2016)571-3.
[37] H.V. Unadkat, M. Hulsman, K. Cornelissen, B.J. Papenburg, R.K. Truckenmuller, G.F. Post, et al. An algorithm-based topographical biomaterials library to instruct cell fate. P Natl Acad Sci USA, 108 (2011)16565-70.
[38] J.K. Hohmann, G. von Freymann. Influence of Direct Laser Written 3D Topographies on Proliferation and Differentiation of Osteoblast-Like Cells: Towards Improved Implant Surfaces. Advanced functional materials, 24 (2014)6573-80.
[39] Y. Lin, Y.M. Shao, J.Y. Li, W.Y. Zhang, K.B. Zheng, X.Y. Zheng, et al. The hierarchical micro-/nanotextured topographies promote the proliferation and angiogenesis-related genes expression in human umbilical vein endothelial cells by initiation of Hedgehog-Gli1 signaling. Artif Cell Nanomed B, 46 (2018)S1141-S51.
[40] A.B. Pardee, D.L. Coppock, H.C. Yang. Regulation of cell proliferation at the onset of DNA synthesis. Journal of cell science Supplement, 4 (1986)171-80.
[41] M. Abbracchio, M. Fumagalli, D. Marangon, G.T. Coppolino, E. Bonfanti, A. Finardi, et al. New mechanisms regulating myelination in the central nervous system: the role of GPR17 and of a novel micro-RNA. J Neurochem, 134 (2015)39-47.

[42] N.G. Gokey, R. Srinivasan, C. Lopez-Anido, C. Krueger, J. Svaren. Developmental Regulation of MicroRNA Expression in Schwann Cells. Molecular and cellular biology, 32 (2012)558-68.
[43] C. Bouquet, M. Ravaille-Veron, F. Propst, F. Nothias. MAP1B coordinates microtubule and actin filament remodeling in adult mouse Schwann cell tips and DRG neuron growth cones. Molecular and cellular neurosciences, 36 (2007)235-47.
[44] L. Lei, L. Tang. Schwann cells genetically modified to express S100A4 increases GAP43 expression in spiral ganglion neurons in vitro. Bioengineered, 8 (2017)404-10.
[45] D.A.a.D.J.F. M. MATA. S100 is preferentially distributed in myelin-forming Schwann cells. Journal of Neurocytotogy, 19 (1990)11-21.
[46] R. Yang, D. Lirussi, T.M. Thornton, D.M. Jelley-Gibbs, S.A. Diehl, L.K. Case, et al. Mitochondrial Ca2+ and membrane potential, an alternative pathway for Interleukin 6 to regulate CD4 cell effector function. eLife, 4 (2015)e06376-88.
[47] D. Van Simaeys, D. Turek, C. Champanhac, J. Vaizer, K. Sefah, J. Zhen, et al. Identification of cell membrane protein stress-induced phosphoprotein 1 as a potential ovarian cancer biomarker using aptamers selected by cell systematic evolution of ligands by exponential enrichment. Analytical chemistry, 86 (2014)4521-7.

Figure legends

Table.1 Oligonucleotide primers used in quantitative real time RT-PCR

Table.2 Percentage of Schwann cells in various cell cycle phases on different samples after 5 day of culture.

Fig.1 Characterization of chitosan micropatterning. (a) SEM observation and water contact angles of chitosan micropatterning with various sizes, A. 10/10 μm, B. 20/20 μm, C. 30/30 μm, D. 50/50 μm. (b) OM observation of the chitosan micropatterning after immersing in PBS for 1、3、5、10、20、30 d, respectively.

Fig.2 Movement and track of Schwann cells on various micropatterned samples and control samples record by time-lapse video. (A, F) 10/10 μm，(B, G) 20/20 μm，(C, H) 30/30 μm，(D, I): 50/50 μm，(E, J) control sample，scale bar=50 μm.

Fig.3 Morphology observation of Schwann cells by TBO staining (a) and immunofluorescence staining (b), respectively, (A) 10/10 μm，(B) 20/20 μm，(C) 30/30 μm，(D) 50/50 μm，(E) control sample. Scale bar=100 μm.

Fig.4 Morphological index of Schwann cells after culture for 1, 3 and 5 days, respectively. (A) Spreading area, *P<0.05 versus other samples. (B) OA, *P<0.05 versus 10/10 μm samples, ND: no detected. (C) Ratio of lateral axis/vertical axis, *P<0.05, **P<0.01 and #P<0.05 compared with 10/10 μm and control samples.

Fig.5 Cell cycle of Schwann cells on various samples measured by flow cytometery after 5 day of culture. (A) 10/10 μm，(B) 20/20 μm，(C) 30/30 μm，(D) 50/50 μm，

(E) control sample.

Fig.6 Protein expression levels of β-catenin and N-cadherin in Schwann cells on various micropatterned samples after 5 days of culture (A). The representative Western blot image is also shown (B). β-actin served as a loading control. Data were presented as means±SD of 3 independent experiments. *P < 0.05 vs. other samples.

Fig.7 Gene expression profiling of morphological-related miRNAs (A) and pathway analysis (B) in micropatterning regulated Schwann cells after culture on 30/30 μm and control sample for 5 days. (C) up/down- regulated genes related various cell biofunction by anisotropic chitosan micropatterning.

Fig.8 The gene expression difference of SCs on chitosan micropatterning and flat control samples after culture for 5 days. *P<0.05 compared with 30/30 μm samples. GAPDH was used as internal reference protein, the data was expressed as mean±SEM, three parallel samples were used for each test.

Fig. 9. Patch clamp measurements for the detection of membrane potential due to morphology variation of Schwann cells on flat and micropatterned sample.

Table.1

Targets	Sequence (5’-3’)
β-actin sense	5'-CCTCTATGCCAACACAGT-3'
β-actin antisense	5'-AGCCACCAATCCACACAG-3'
Smad6 sense	5'-TACCACTTCAGCCGGCTCTG-3'
Smad6 antisense	5'-AGTACGCCACGCTGCACCAGT-3'
MBP sense	5'-AGAGTCCGACGAGCTTCAGA-3'
MBP antisense	5'-CAGGTACTTGGATCGCTGTG-3'
S100 sense	5'-GTTGCCCTCATTGATGTCT-3'
S100 antisense	5'-CTGCTCTTTGATTTCCTCC-3'
Sox10 sense	5'-GAGGAACCTCGCTGCCTGTC-3'
Sox10 antisense	5'-CCGGGAACTTGTCATCGTCTG-3'
MPZ sense	5'-TCTCAGGTCACGCTCTATGTC-3'
MPZ antisense	5'-GCCAGCAGTACCGAATCAG-3'
GAPDH sense	5'-GCAAGTTCAACGGCACAG-3'
GAPDH antisense	5'- CGCCAGTAGACTCCACGAC -3'

Table.2

Sample	Phase		
	G1 (%)	G2 (%)	S (%)
10/10 μm	80.6	13	6.4
20/20 μm	81.59	12.52	5.9
30/30 μm	78.49	13.53	7.98
50/50 μm	80.75	13.41	5.94
Control	77.67	12.74	9.59

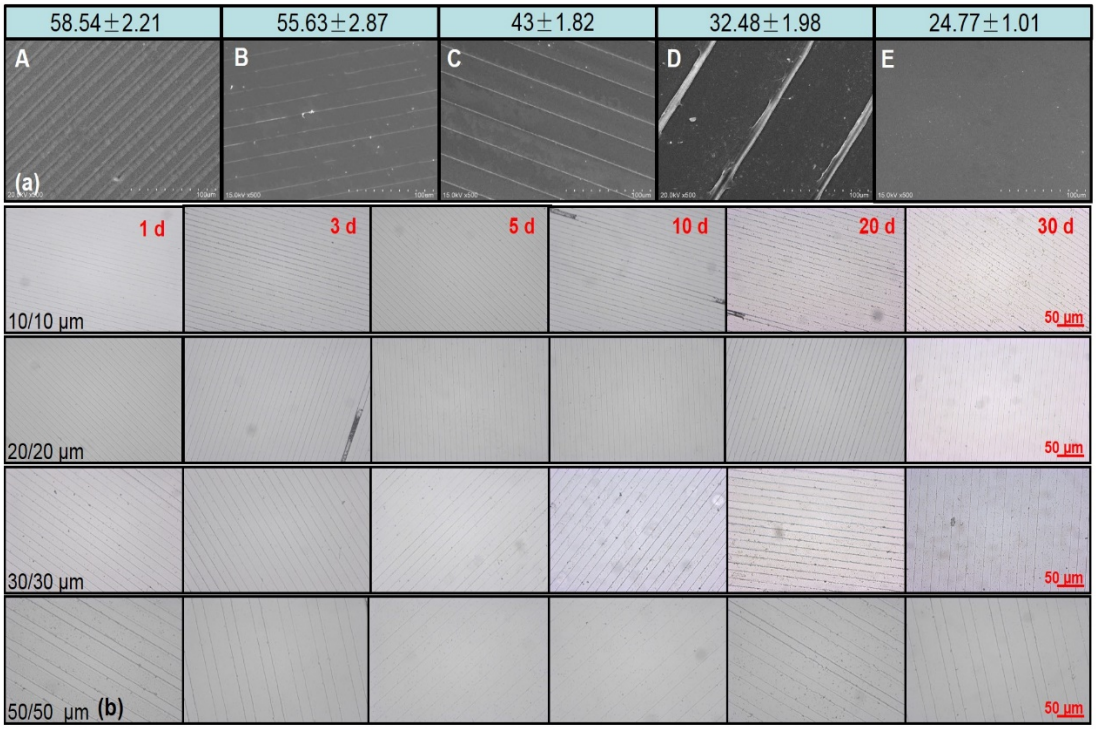
58.54±2.21
55.63±2.87
43±1.82
32.48±1.98
24.77±1.01
A
B
C
D
E
(a)
1 d
3 d
5 d
10 d
20 d
30 d
10/10 μm
20/20 μm
30/30 μm
50/50 μm (b)
50 μm

Fig.1

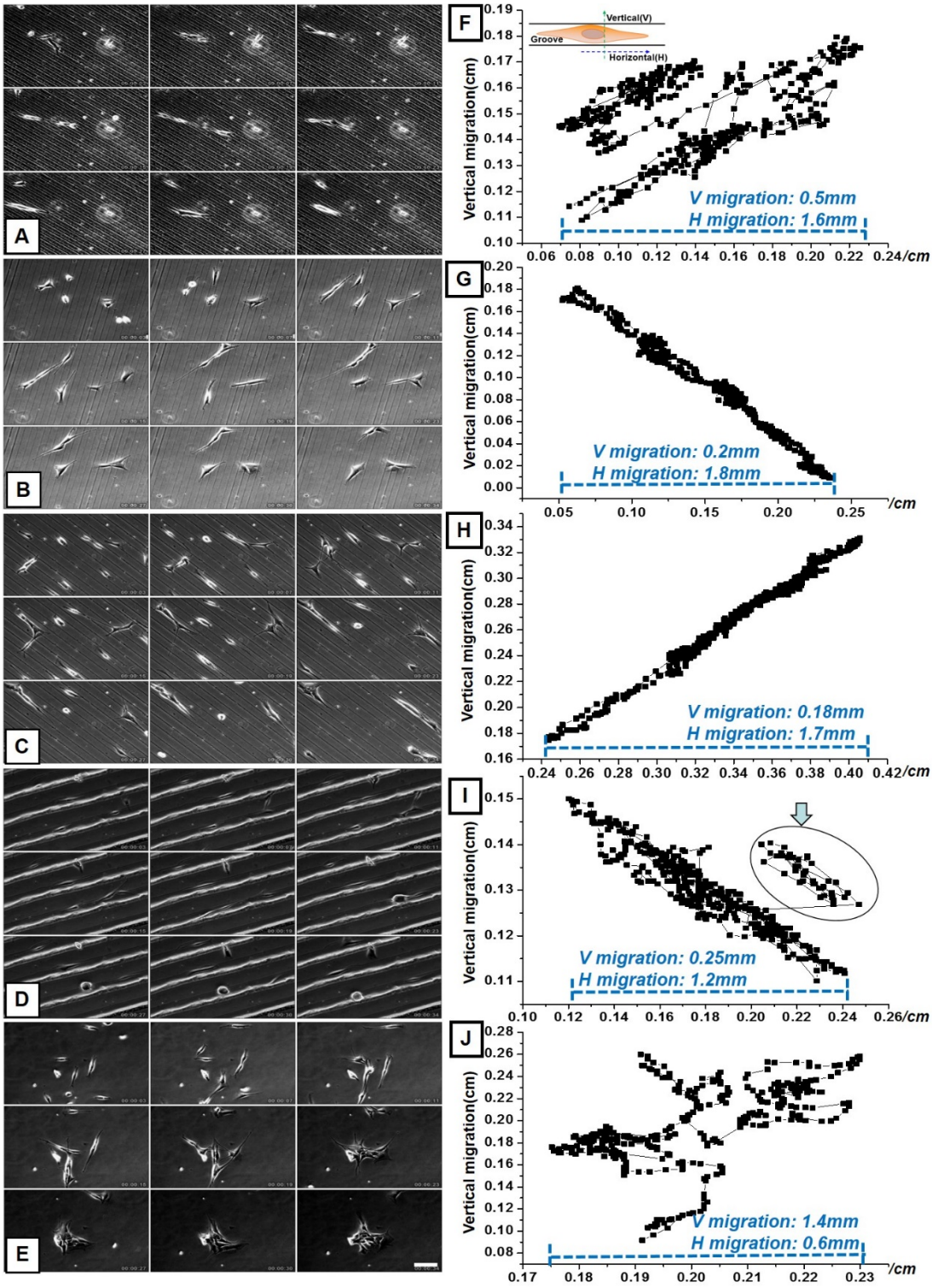
A
B
C
D
E
F
Vertical(V)
Groove
Horizontal(H)
Vertical migration(cm)
V migration: 0.5mm
H migration: 1.6mm
/cm
G
V migration: 0.2mm
H migration: 1.8mm
H
V migration: 0.18mm
H migration: 1.7mm
I
V migration: 0.25mm
H migration: 1.2mm
J
V migration: 1.4mm
H migration: 0.6mm

Fig.2

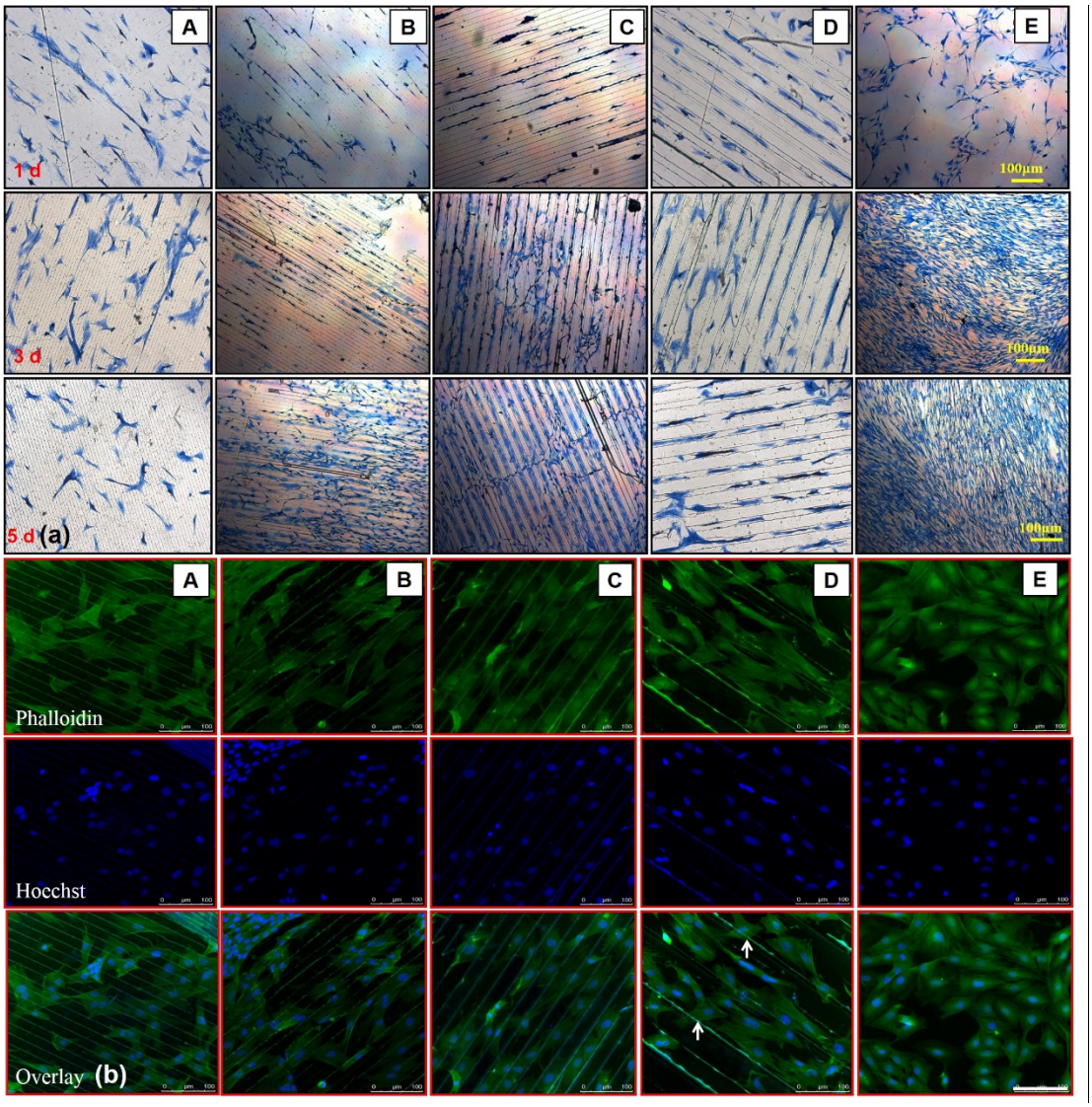
A
B
C
D
E
1 d
100μm
3 d
100μm
5 d (a)
100μm
A
B
C
D
E
Phalloidin
Hocchst
Overlay (b)

Fig.3

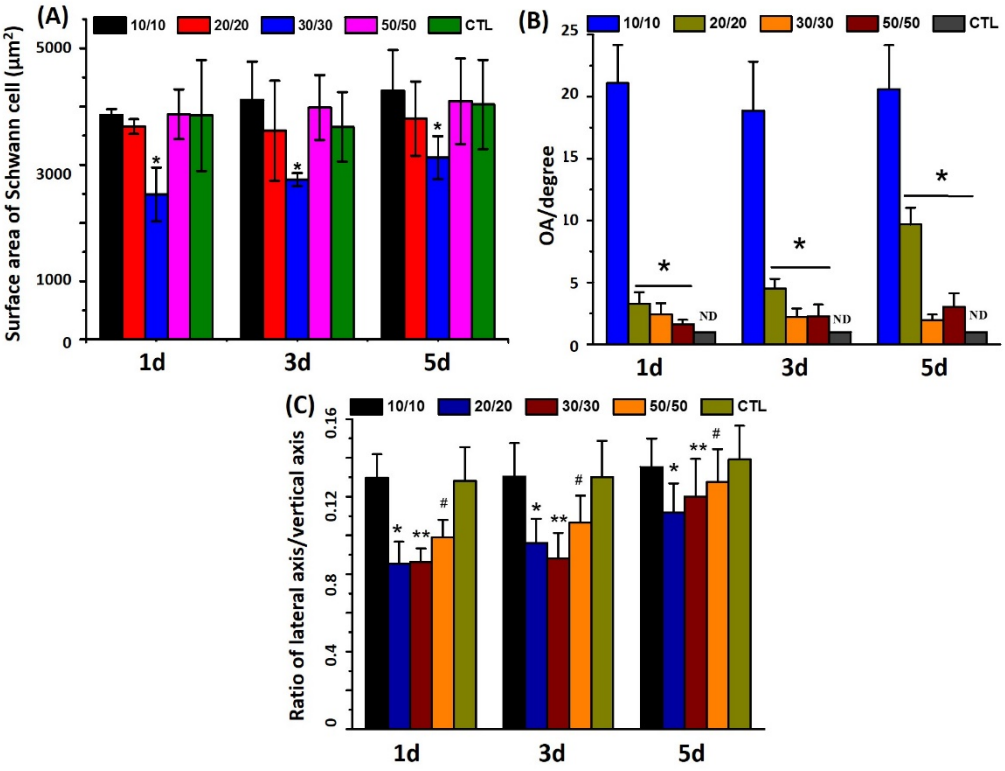
(A)
10/10
20/20
30/30
50/50
CTL
Surface area of Schwann cell (μm²)
5000
3000
1000
0
1d
3d
5d
(B)
10/10
20/20
30/30
50/50
CTL
OA/degree
25
20
15
10
5
0
ND
1d
3d
5d
(C)
10/10
20/20
30/30
50/50
CTL
Ratio of lateral axis/vertical axis
0.16
0.12
0.8
0.4
0
1d
3d
5d

Fig.4

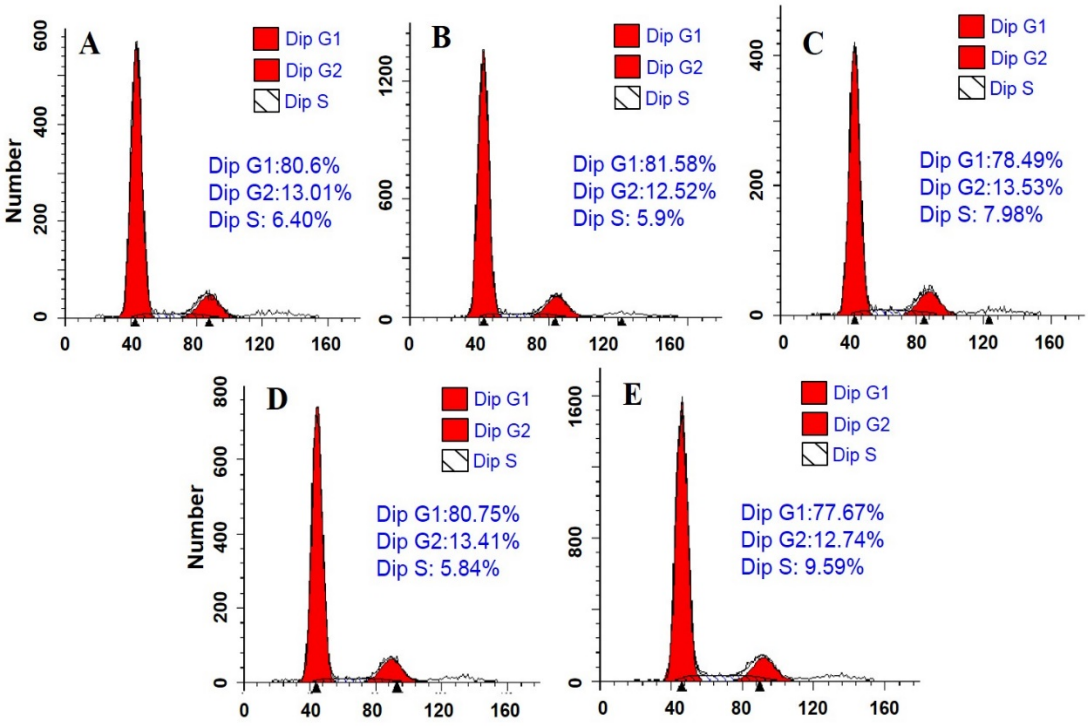
A
Dip G1
Dip G2
Dip S
Dip G1:80.6%
Dip G2:13.01%
Dip S: 6.40%
Number
B
Dip G1
Dip G2
Dip S
Dip G1:81.58%
Dip G2:12.52%
Dip S: 5.9%
C
Dip G1
Dip G2
Dip S
Dip G1:78.49%
Dip G2:13.53%
Dip S: 7.98%
D
Dip G1
Dip G2
Dip S
Dip G1:80.75%
Dip G2:13.41%
Dip S: 5.84%
Number
E
Dip G1
Dip G2
Dip S
Dip G1:77.67%
Dip G2:12.74%
Dip S: 9.59%

Fig.5

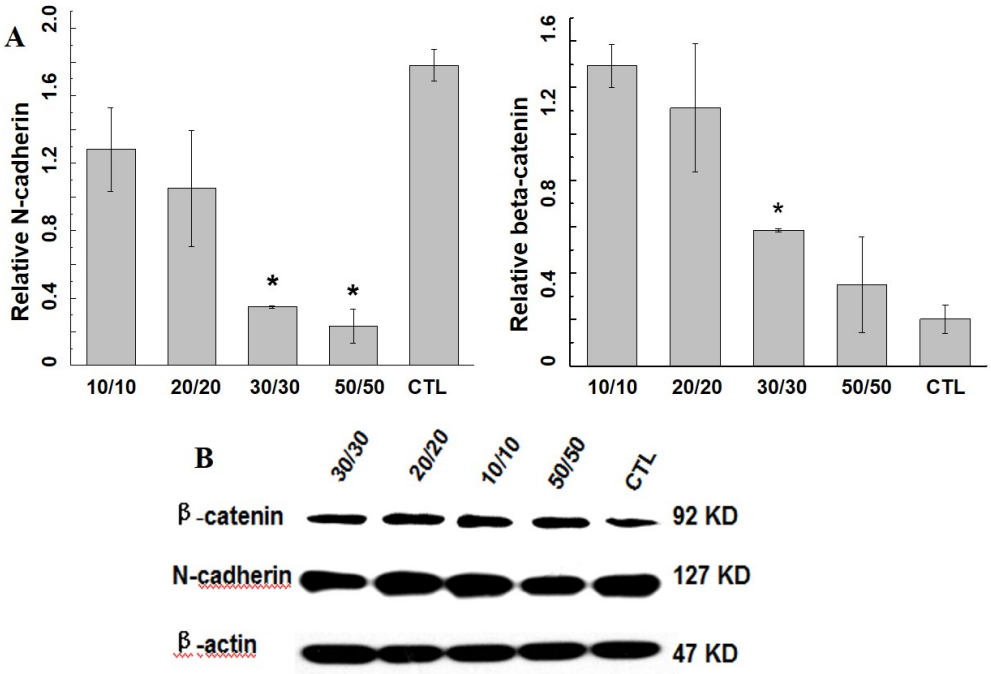
A
Relative N-cadherin
0
0.4
0.8
1.2
1.6
2.0
10/10
20/20
30/30
50/50
CTL
*
*
Relative beta-catenin
0
0.4
0.8
1.2
1.6
10/10
20/20
30/30
50/50
CTL
*
B
30/30
20/20
10/10
50/50
CTL
β-catenin
92 KD
N-cadherin
127 KD
β-actin
47 KD

Fig.6

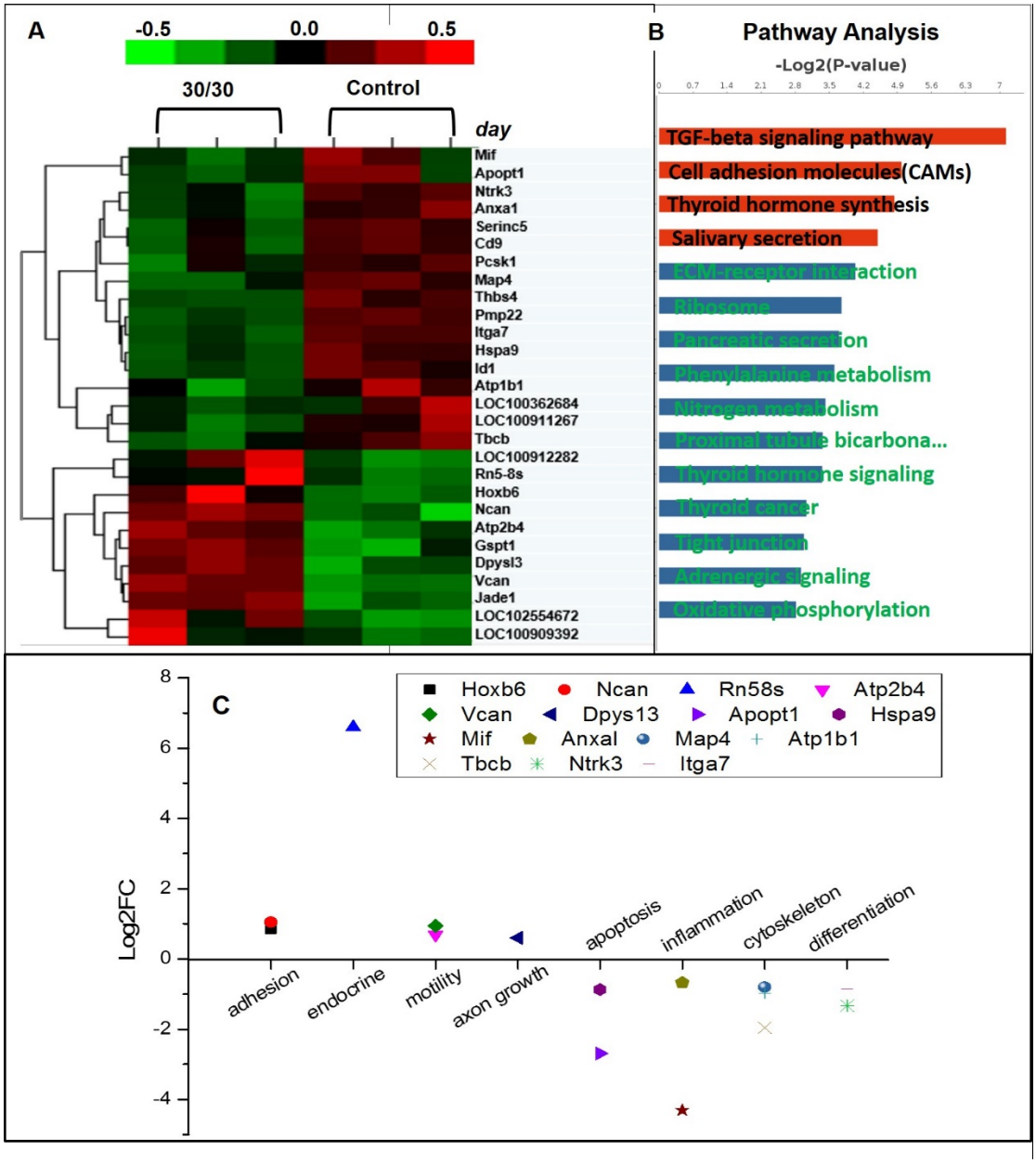
A
-0.5
0.0
0.5
30/30
Control
day
Mif
Apopt1
Ntrk3
Anxa1
Serinc5
Cd9
Pcsk1
Map4
Thbs4
Pmp22
Itga7
Hspa9
Id1
Atp1b1
LOC100362684
LOC100911267
Tbcb
LOC100912282
Rn5-8s
Hoxb6
Ncan
Atp2b4
Gspt1
Dpysl3
Vcan
Jade1
LOC102554672
LOC100909392
B
Pathway Analysis
-Log2(P-value)
0
0.7
1.4
2.1
2.8
3.5
4.2
4.9
5.6
6.3
7
TGF-beta signaling pathway
Cell adhesion molecules(CAMs)
Thyroid hormone synthesis
Salivary secretion
ECM-receptor interaction
Ribosome
Pancreatic secretion
Phenylalanine metabolism
Nitrogen metabolism
Proximal tubule bicarbona...
Thyroid hormone signaling
Thyroid cancer
Tight junction
Adrenergic signaling
Oxidative phosphorylation
C
Hoxb6
Ncan
Rn58s
Atp2b4
Vcan
Dpys13
Apopt1
Hspa9
Mif
Anxal
Map4
Atp1b1
Tbcb
Ntrk3
Itga7
Log2FC
8
6
4
2
0
-2
-4
adhesion
endocrine
motility
axon growth
apoptosis
inflammation
cytoskeleton
differentiation

Fig.7

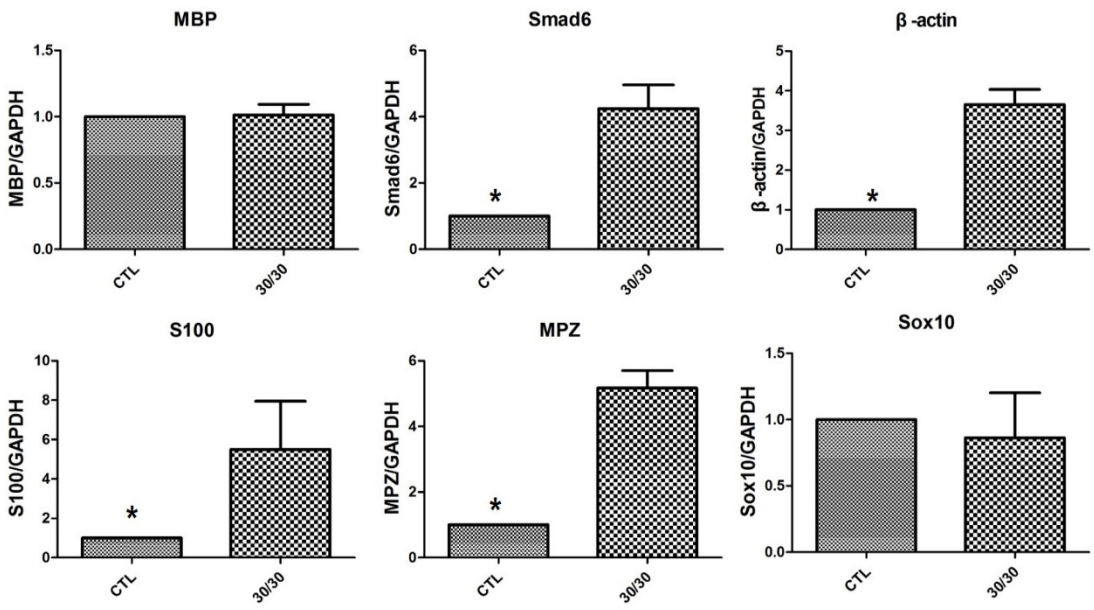
MBP
MBP/GAPDH
1.5
1.0
0.5
0.0
CTL
30/30
Smad6
Smad6/GAPDH
6
4
2
0
*
CTL
30/30
β -actin
β -actin/GAPDH
5
4
3
2
1
0
*
CTL
30/30
S100
S100/GAPDH
10
8
6
4
2
0
*
CTL
30/30
MPZ
MPZ/GAPDH
6
4
2
0
*
CTL
30/30
Sox10
Sox10/GAPDH
1.5
1.0
0.5
0.0
CTL
30/30

Fig.8

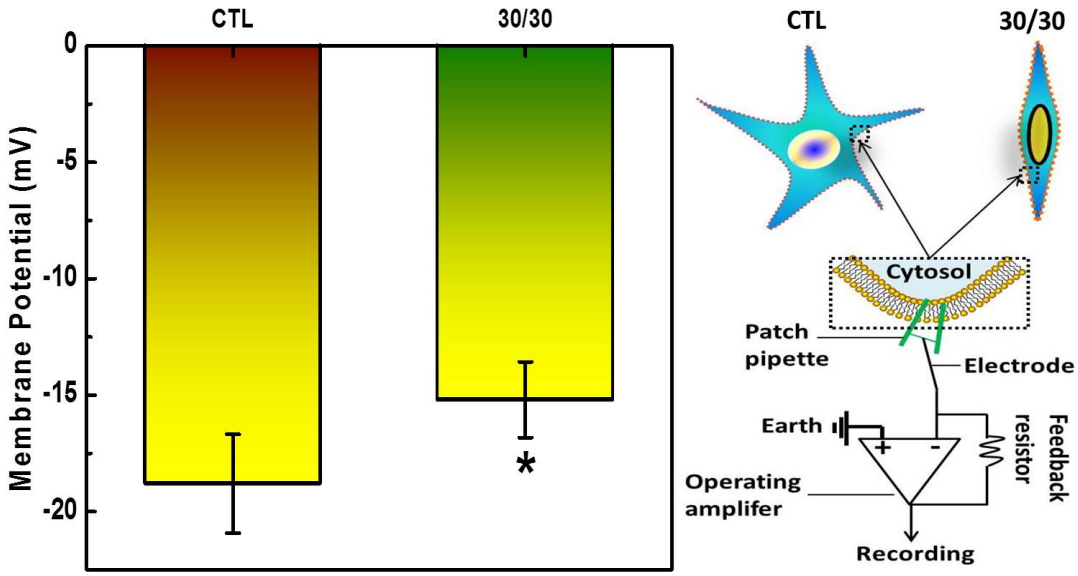
CTL
30/30
0
-5
-10
-15
-20
Membrane Potential (mV)
*
CTL
30/30
Cytosol
Patch
pipette
Electrode
Earth
+
-
Feedback
resistor
Operating
amplifer
Recording

Fig. 9